



LAWRENCE  
LIVERMORE  
NATIONAL  
LABORATORY

# Source Characterization of the August 6, 2007 Crandall Canyon Mine Seismic Event in Central Utah

S. R. Ford, D. S. Dreger, W. R. Walter

November 16, 2007

Seismological Research Letters

## **Disclaimer**

---

This document was prepared as an account of work sponsored by an agency of the United States government. Neither the United States government nor Lawrence Livermore National Security, LLC, nor any of their employees makes any warranty, expressed or implied, or assumes any legal liability or responsibility for the accuracy, completeness, or usefulness of any information, apparatus, product, or process disclosed, or represents that its use would not infringe privately owned rights. Reference herein to any specific commercial product, process, or service by trade name, trademark, manufacturer, or otherwise does not necessarily constitute or imply its endorsement, recommendation, or favoring by the United States government or Lawrence Livermore National Security, LLC. The views and opinions of authors expressed herein do not necessarily state or reflect those of the United States government or Lawrence Livermore National Security, LLC, and shall not be used for advertising or product endorsement purposes.

# Source Characterization of the August 6, 2007 Crandall Canyon Mine Seismic Event in Central Utah

S. R. Ford<sup>1,2</sup>, D. S. Dreger<sup>1</sup>, and W. R. Walter<sup>2</sup>

## SUMMARY

On August 6, 2007 a local magnitude 3.9 seismic event occurred at 08:48:40 UTC in central Utah. The epicenter is within the boundaries of the Crandall Canyon coal mine (c.f. Pechmann et al., this volume). We performed a moment tensor analysis with complete, three-component seismic recordings from stations operated by the USGS, the University of Utah, and EarthScope. The analysis method inverts the seismic records to retrieve the full seismic moment tensor, which allows for interpretation of both shearing (e.g., earthquakes) and volume-changing (e.g., explosions and collapses) seismic events. The results show that most of the recorded seismic wave energy is consistent with an underground collapse in the mine. We contrast the waveforms and moment tensor results of the Crandall Canyon Mine seismic event to a similar sized tectonic earthquake about 200 km away near Tremonton, Utah, that occurred on September 1, 2007. Our study does not address the actual cause of the mine collapse.

## INTRODUCTION

In this paper we apply the moment tensor analysis techniques described in Ford et al. (2007) to improve our understanding of the source of the seismic waves for two very different recent events in Utah. Ford et al (2007) implement the time-domain full regional waveform inversion for the complete moment tensor (2nd rank tensor,  $M_{ij}$ ) devised by Minson and Dreger (2007) after Herrmann and Hutchenson (1993) based on the work of Langston (1981). Moment tensors are determined by matching synthetic seismograms to data at periods where the Earth can be characterized by a simple plane layer model. The complete moment tensor allows for a characterization of the relative amounts of deviatoric and isotropic ( $M_{ij}$  where  $i=j$ ) source components, and a constraint on the source depth. The isotropic component is related to the volume change associated with a source (Muller, 1973), and in the case of a collapse this volume change is expected to be significant.

In general, synthetic seismograms are represented as the linear combination of fundamental Green's functions where the weights on these Green's functions are the individual moment tensor elements. The Green's functions for a one-dimensional (1-D) velocity model of eastern California and western Nevada (Table 1; Song et al., 1996) are calculated as synthetic displacement seismograms using a frequency-wavenumber integration method (Saikia, 1994). The synthetic data is filtered with a 4-pole acausal Butterworth filter with a low-corner of 0.02 Hz and a high-corner of 0.1 Hz (10-50s period). The high corner of the filter was chosen so as to achieve a good signal-to-noise ratio while keeping it low enough to assume a point-source at the wavelengths investigated. The low corner was chosen empirically and for stability. At these frequencies, where the dominant wavelengths are approximately 30 to 150 km, we assume a point source for the low-magnitude regional events investigated in this study. The point source assumption allows for linearization in the time-domain, which is where we carry out the least-squares inversion. The data is processed by removing the instrument response, rotating to the

great-circle frame of reference, integrating to obtain displacement, and filtering to the same frequency band as the synthetic seismograms.

The broadband stations from the USGS, the University of Utah and EarthScope's USArray networks provide excellent azimuthal coverage of the event at the Crandall Canyon Mine in central Utah on August 6, 2007. Over 200 stations recorded this event well, and we choose three-component data from the 16 best stations, based on signal to noise level and azimuthal coverage to perform the inversion. We will compare the Crandall Canyon Mine event results with those from an earthquake about 200 km to the north that occurred on September 1, 2007 near Tremonton, Utah. Figure 1 shows the locations of the events and stations used in the inversions.

## ANALYSIS

The Green's functions for the Crandall Canyon Mine event were calculated at a depth of 1 km, consistent with the shallow depth reported for this event. We will test this assumption in a later section. The best-fit moment tensor has a total scalar seismic moment of 2.12 mAk (The 2007 IUGG/IASPEI General Assembly in Perugia, Italy recommends  $10^{18}$  N-m equal 1 Aki [Ak], so that 2.12 mAk is  $2.12 \times 10^{15}$  N-m), corresponding to a moment magnitude ( $M_w$ ) of 4.15. The mechanism is one that is dominated by implosive isotropic energy, and predicts dilational (down) first-motions at all azimuths as shown in Figure 2a. The waveform fits to the data using this mechanism are excellent as shown in Figure 3 and give a 54.1% variance reduction (VR), where 100% VR is perfect fit. We compare this mechanism with one obtained for the earthquake near Tremonton, Utah. For the Tremonton event the depth that produced the best fit is 9 km and the mechanism is dominantly double-couple (DC) with a  $M_w$  of 3.7 as shown in Figure 2b. Waveform fits are excellent as shown in Figure 4, with a 65.7% VR. In contrast to the Crandall Canyon Mine event, this mechanism predicts both compressional and dilational P-wave first motions.

We compare the best-fit mechanism for the Crandall Canyon Mine event with other potential mechanisms using the best six stations (Figure 5). As with the 16-station analysis, the full solution provides a good fit to the data (with an improved VR of 72.8%). We also calculate the best-fit deviatoric solution, which zeros out the isotropic component by setting  $M_{zz} = -(M_{xx} + M_{yy})$ . The deviatoric solution fits the data poorly (VR of 41.8%) and does not adequately produce energy on the radial and vertical traces to fit the data, especially at the nodal station DUG. We also test a best-fit pure closing crack with the axis in the horizontal plane, or a horizontal closing crack. The isotropic moment of this best-fit closing crack is equal to the isotropic moment of the full solution. Contrary to the observations, this mechanism does not produce any Love waves. Finally, we test a typical 6 km deep Basin & Range normal mechanism that has the strike of the nearby Joe's Valley Fault, and where the  $M_0$  is chosen to best fit the data. At some stations the waveforms predicted by this mechanism are completely out of phase with the data. This effect is easily seen when comparing the Love and Rayleigh wave radiation patterns predicted by these potential mechanisms as shown in Figure 6 for a distance of 300 km. The Basin & Range mechanism predicts Love waves that are of opposite polarity than that predicted for the full solution at DUG. The deviatoric solution predicts almost no Rayleigh waves at stations DUG and Q18A, and significant amplitude and phase mismatches of Rayleigh waves at other stations.

It is difficult to grasp the source-type from the standard focal mechanism plot. For example, one cannot discern the relative contributions of the isotropic and deviatoric components from the full focal mechanism in Figure 2a. In addition, decompositions of the deviatoric component are non-unique (Julian et al., 1998), and will be discussed later. Following the source-type analysis described in Hudson et al. (1989), and as employed by Ford et al. (2007), we calculate  $-2\varepsilon$  and  $k$ , which are given by

$$\varepsilon = \frac{-m'_1}{|m'_3|}, \quad (1)$$

and

$$k = \frac{M_{\text{ISO}}}{|M_{\text{ISO}}| + |m'_3|}, \quad (2)$$

where  $m'_1$ ,  $m'_2$  and  $m'_3$  are the deviatoric principal moments for the T, N, and P axes, respectively, and  $M_{\text{ISO}} = \text{trace}(M_{ij})/3$ .  $\varepsilon$  is a measure of the departure of the deviatoric component from a pure double-couple mechanism, and is 0 for a pure double-couple and  $\pm 0.5$  for a pure compensated linear vector dipole (CLVD).  $k$  is a measure of the volume change, where +1 would be a full explosion and  $-1$  a full implosion. We calculate  $-2\varepsilon$  and  $k$  for the Crandall Canyon Mine and Tremonton events and present them on the source-type plot in Figure 7. The projection used in the source-type plot is designed so as to make the parameter variance linear for the moment tensor elements. The Crandall Canyon Mine event plots very near the point for a theoretical closing crack mechanism or anti-crack in a Poisson solid, which represents the process of collapse of an underground cavity (Pechmann et al., 1995; Bowers and Walter, 2002). The Tremonton event plots near the origin, which is consistent with a DC tectonic event. The source-type parameters from two past mine collapses in the Trona mine area of Wyoming and one explosion cavity collapse at the Nevada Test Site (NTS) along with the NTS nuclear test explosion, BEXAR, are also given from the analysis of Ford et al. (2007) for comparison. The other collapse events are also located in the region of the plot near a pure closing crack and near the Crandall Canyon Mine event.

## DEPTH SENSITIVITY

Analysis of the sensitivity of the moment tensor solution to source depth indicates that shallow depths are preferred (Figure 8). In this analysis 16 stations were used and the data was processed as described above. Depths of 600m, 800m and 1 km gave similar levels of fit. The slight improvement in fit from 2 to 3 km depth is likely due to the presence of a velocity discontinuity in the structure modeled used to compute the Green's functions (Table 1). The moment tensor solution remains stable and strongly crack-like over the depth range from 600 m to 5 km. Assumed sources at greater than 5 km depth become less crack-like, but remain substantially different from a double-couple.

## SOURCE DECOMPOSITION

Previous work modeling intermediate period (10-50s) seismic waveforms has shown the sudden collapse of underground cavities is well modeled using a vertically closing crack model (e.g., Pechmann et al., 1995; Bowers and Walter, 2002). For example the collapse of an approximately two square kilometer area of the Solvay trona mine in Wyoming on February 3, 1995 generated an  $M_L$  5.2 seismic event. Intermediate surface waves and short period first motion data were nicely fit using a closing tensile crack moment tensor, and were inconsistent with earthquake DC mechanisms (Pechmann et al, 1995). This 1995 event and a subsequent collapse event in 2000 are the green colored reference points near the closing (negative) crack location in Figure 7. For sources near the surface of the Earth one can show that a related model for cavity collapses: a block dropping vertically downward represented as vertical point forces (Taylor, 1994), produces basically the same waveforms as the closing crack model (Day and McLaughlin, 1991; Bowers and Walter, 2002).

The simple closing crack representation allows an estimate of the area of the mine collapse from the seismic data alone, analogous to the ability to estimate the rupture area of a purely DC earthquake from its point source moment. In the case of the gravity driven, horizontally lying vertical closing crack, the moment is given by

$$M_{xx} = M_{yy} = -\lambda S\bar{u} \quad \text{and} \quad M_{zz} = -(\lambda + 2\mu) S\bar{u} \quad (3)$$

where  $\lambda$  and  $\mu$  are Lamé parameters,  $S$  is the area of the crack and  $\bar{u}$  is the average closure distance. Once we have a waveform based moment and an estimate of the average closure distance, we can seismically determine the collapse area.

The damaged region in the Crandall Canyon coal mine has a room and pillar configuration ([www.msha.gov/Genwal/CrandallCanyon.asp](http://www.msha.gov/Genwal/CrandallCanyon.asp)), where parts of the coal seam are removed and portions are left as pillars to support the roof in a grid-like pattern. Typically room and pillar mines have an “extraction rate” for the percent of material removed. In a mine with 50% extraction the largest possible closure would be half the pillar height, if the mined material had the same density as the original seam after collapse. However, the pillar material will fracture and rubblize in the collapse (called the “swell”), so the actual closure distance will be less. For example in the February 3, 1995 Wyoming mine collapse, which occurred in an approximately 60% extraction room and pillar section of a trona mine, the average closure distance determined from both the seismic moment and the surface subsidence was about 0.6 m (Pechmann et al, 1995). This distance was between one fourth and one fifth of the original pillar height of 2.8m.

In the case of the Crandall Canyon mine, Pechmann et al. (this volume) estimated the extraction rate in the vicinity of the collapse to be between approximately 35 and 45%. They also give the pillar height as 2.4 m and estimate the coal to swell between 40 and 50%. Under the assumptions that pillars are entirely rubblized, such that any remaining air space after collapse is accounted for by the swell, and the area under consideration does not change, we can derive a formula for the closure distance,  $\bar{u}$ , in terms of the original pillar height  $h$ , the extraction fraction  $e$ , and the swell fraction  $s$  as:

$$\bar{u} = h[1 - (1 - e)(1 + s)]. \quad (4)$$

This leads to estimates of the closure distance of 0.06 to 0.55 m. We can decompose the full moment tensor ( $M^{\text{full}}$ ) for the Crandall Canyon Mine event into the simple gravity driven collapse model (represented as a horizontal closing crack;  $M^{\text{crack}}$ ) plus smaller secondary components contained in a remainder moment tensor ( $M^{\text{rem}}$ ), or

$$M^{\text{full}} = M^{\text{crack}} + M^{\text{rem}}. \quad (5)$$

We estimate the Lamé parameters from the velocity model used to calculate the Green's functions for the inversion so that  $\lambda = 1.0 \times 10^{10}$  Pa. In this case the Poisson's ratio ( $\nu$ ) is 0.26 and the  $M^{\text{crack}}$  moment ratio is [1:1:2.85]. The moment associated with the volume change ( $S\bar{u}$ ) is selected so as to remove the isotropic component in  $M^{\text{rem}}$ , which is to say that all volumetric change is due to the collapse. In matrix form (5) becomes

$$\begin{bmatrix} -55.24 & -10.51 & 20.51 \\ -10.51 & -54.16 & 26.55 \\ 20.51 & 26.55 & -182.50 \end{bmatrix} = \begin{bmatrix} -60.25 & 0 & 0 \\ 0 & -60.25 & 0 \\ 0 & 0 & -171.40 \end{bmatrix} + \begin{bmatrix} 5.01 & -10.51 & 20.51 \\ -10.51 & 6.09 & 26.55 \\ 20.51 & 26.55 & -11.10 \end{bmatrix} \quad (6)$$

where each moment is in units of  $10^{-5}$  Ak ( $10^{13}$  N-m). In this case  $M^{\text{rem}}$  represents only 22% of the total moment in  $M^{\text{full}}$ , and the closing crack  $M_{xx}$  moment tensor component is  $6.03 \times 10^{14}$  N-m. Using the range 0.06 to 0.55 m for the closure distance, we estimate the collapse area to be about 1.1 to  $10.0 \times 10^5$  m<sup>2</sup>. If square, this area would be approximately 330 to 1000 m on a side. Small closure distances lead to unrealistically large collapse areas, so we favor solutions near the larger closure distance and the smaller collapse area.

As can be seen in Figure 3, there is substantial Love wave energy at all stations, which cannot be produced from a purely gravity-driven closing crack as analyzed above. We investigate the source of this anomalous energy through an exercise in non-unique decompositions in the form of (5), where we remove the pure collapse mechanism and examine the remainder. We try two different types of decompositions, the first using the remainder as given in (6) and a second decomposition where we allow the  $\nu$  to vary.

We test two non-unique decompositions of the remainder,  $M^{\text{rem}}$  given by (6). The first decomposition splits  $M^{\text{rem}}$  into to a DC and CLVD mechanism that share the same P and T axes as shown in Figure 9a. This results in a small DC component and a large CLVD component where the largest principle moment is 73% of the largest principle moment of  $M^{\text{rem}}$ . We note that Fletcher and McGarr (2005) present full moment tensor results for 6 small ( $1.3 < M < 1.8$ ) mining-induced seismic events in the Trail Mt. region of Utah about 15 km south of the Crandall Canyon Mine event. Decomposition of those events in the same manner (using a horizontal crack that leaves no isotropic remainder with a Poisson ratio ( $\nu=0.25$ ) defined by their Green's function velocity model parameters) also produces significant non-DC components. If one assumes a remainder split into DC and CLVD that share the P and T axes, then half of the Fletcher and McGarr (2005) events also have a majority CLVD component in the remainder.

The same  $M^{\text{rem}}$  from (6) can also be decomposed to a major and minor DC as shown in Figure 9b. In this case the largest principle moment of the major DC is the largest principle moment of

$M^{\text{rem}}$ , and the largest principle moment of the minor DC is the smallest principle moment of  $M^{\text{rem}}$ , so that the moment of the minor DC is 36% of the major DC. This decomposition produces mechanisms with different T and P axes. Interpretations of these non-unique decompositions are themselves non-unique. A simplistic and speculative possibility in the case of the large CLVD remainder could be that it is associated with non-volumetric redistribution of material within the mine following the collapse, or additional elastic relaxation near the mine due to non-uniform stress. In the major DC remainder case (Figure 9b) an interpretation might be that the collapse was uneven so that portions of the closure were accommodated by a large nearly vertical block motion on one side of the collapse. Alternatively the large DC remainder could represent shear between the floor and roof of the cavity. In both cases we might assume the smallest DC remainder could simply come from noise in the data and errors in the Green function compared to the true Earth structure.

The second type of decomposition allows the Poisson ratio and volume change to vary so that  $M^{\text{rem}}$  is purely DC. This occurs when  $\nu = 0.18$  giving a  $M^{\text{crack}}$  moment ratio [1:1:4.56] so that (4) is given by

$$\begin{bmatrix} -55.24 & -10.51 & 20.51 \\ -10.51 & -54.16 & 26.55 \\ 20.51 & 26.55 & -182.50 \end{bmatrix} = \begin{bmatrix} -44.53 & 0 & 0 \\ 0 & -44.53 & 0 \\ 0 & 0 & -202.85 \end{bmatrix} + \begin{bmatrix} -10.71 & -10.51 & 20.51 \\ -10.51 & -9.63 & 26.55 \\ 20.51 & 26.55 & 20.35 \end{bmatrix} \quad (7)$$

where each moment is in units of  $10^{-5} \text{ Ak}$  ( $10^{13} \text{ N-m}$ ). In this case  $M^{\text{rem}}$  represents only 21% of the total moment in  $M^{\text{full}}$ , and the closing crack  $M_{xx}$  moment tensor component is  $4.45 \times 10^{14} \text{ N-m}$ . If we assume that  $\lambda$  and  $\bar{u}$  are the same, the collapse area is approximately 280 to 860 m on a side and  $M^{\text{rem}}$  would be given by Figure 9c. It is interesting to note that the  $M^{\text{rem}}$  mechanism in this decomposition is the same as the deviatoric inversion results shown in Figure 5. As we discussed in the previous case with the DC remainder this mechanism could be consistent with an uneven collapse of the cavity accommodated by normal mechanism style block motion above part of the cavity. This could be related to asymmetric in-situ stresses in the region from a variety of possible source such as topography, tectonic forces and mining-related changes. Finally we note that the second decomposition gives a low Poisson ratio that is inconsistent with the velocity model used in the inversion or with the intact coal or sedimentary rocks in the region. Recalculation of the moment tensor using a velocity model with a 500 m strip at the source depth of decreased  $V_\alpha$  that is consistent with the inferred  $\nu$  does not result in a decomposition similar to (7). Therefore, a speculative interpretation would be that the low Poisson ratio is a local effect related to the damaged rock in the immediate region of the mine collapse. Another explanation of the greater vertical to horizontal moment ratio than specified by the Green's functions is that it is a manifestation of over-closure of the crack due to inelastic accommodation afforded by a secondary vertical dip-slip source. The conjugate fault of the DC given by  $M^{\text{rem}}$  in (7) and shown in Figure 9c (strike =  $303^\circ$ , rake =  $73^\circ$ , dip =  $16^\circ$ ) suggests another alternate scenario, which is differential shear between the roof and floor of the mine along a southwesterly trajectory.

The decompositions discussed in this section are non-unique and the interpretations associated with them are speculative. Our intent here was to cover the range of possibilities for the secondary source. However one should not lose sight of the fact that the primary and dominant

source for this event is a closing crack mechanism (78 and 79% of the total moment for the two decomposition types), which is consistent with the observed collapse in the mine and with that observed in previous large cavity collapse seismic events in the Western U.S. (e.g., Taylor et al 1994; Pechmann et al.; 1995, Bowers and Walter, 2002). As the comparison with the September 1, 2007 Tremonton earthquake and many other western U.S. earthquakes analyzed in Ford et al. (2007) show, the Crandall Canyon Mine event is not consistent with a tectonic earthquake. The cause of the significant secondary shear source associated with this event remains poorly understood and perhaps differentiates this mine collapse from some of the previous ones analyzed. Significant work remains to be done to reconcile the collapse area implied by the seismic event and the causes of the secondary shear source with the details of what occurred in the mine itself and warrant further investigation that is beyond the scope of this paper.

## CONCLUSIONS

The local magnitude 3.9 Crandall Canyon Mine seismic event that occurred in central Utah on August 6, 2007 is significantly different from the similar size earthquake that occurred near Tremonton, Utah on September 1, 2007. Full moment tensor analysis shows the Crandall Canyon Mine event is most consistent with previous shallow cavity collapse events that have a closing crack mechanism, and is quite different from typical tectonic earthquakes at depths of 5-15 km. This interpretation is robust to small errors in the source depth, and a non-DC mechanism is retrieved at all depths. Mechanisms that have no volume-change and typical Basin & Range normal focal mechanism do not fit the observed waveforms. However, a purely vertically closing, horizontally lying crack cannot explain the large Love wave observations, and an additional shear mechanism is needed to fully explain the observed waveforms. Such a mechanism could be explained by an asymmetric collapse of the mine cavity due to unevenly distributed in-situ stresses, sympathetic shear on a roof fault, or between the roof and floor of the mine, and warrants further investigation.

## ACKNOWLEDGEMENTS

Data was collected from the BUD Data Center of IRIS with the program JWeed. This work is done under Department of Energy BAA contract DE-FC52-06NA27324 and in part under the auspices of the U.S. Department of Energy by University of California, Lawrence Livermore National Laboratory under Contract W-7405-Eng-48. This is LLNL contribution # and BSL contribution #. Signal processing was done with SAC, and figures were made with GMT.

## REFERENCES

- Bowers, D and W. R. Walter, (2002), Discriminating between large mine collapses and explosions using teleseismic P waves, *Pure. Appl. Geophys.*, 159, 803-830.
- Day, S. M. and K. L. McLaughlin (1991), Seismic source representations for spall, *Bull. Seism. Soc. Am.*, 81, 191-201.
- Dreger, D. and B. Woods (2002). Regional distance seismic moment tensors of nuclear explosions; seismic source mechanism through moment tensors, *Tectonophysics*, 356(1-3), 139-156.
- Fletcher, J.B. and A. McGarr (2005), Moment Tensor Inversion of Ground Motion from Mining-Induced Earthquakes, Trail Mountain, Utah, *Bull. Seis. Soc. Am.*, 95, 48-57.
- Ford, S.R., Douglas S. Dreger, and William R. Walter (2007) Identifying isotropic events using an improved regional moment tensor inversion technique, Monitoring Research Review, Denver, CO.
- Herrmann, R. B. and K. Hutchensen (1993). Quantification of MLg for small explosion, Tech. rep., Phillips Laboratory Report PL-TR-93-2070.
- Hudson, J. A., R. G. Pearce, R. G., and R. M. Rogers (1989). Source type plot for inversion of the moment tensor, *J. Geophys. Res.*, 9(B1), 765-774.
- Julian, B. R., A. D. Miller and G. R. Foulger (1998). Non-double-couple earthquakes; 1. Theory, *Rev. Geophysics*, 36(4), 525- 549.
- Langston, C. A. (1981). Source inversion of seismic waveforms; the Koyna, India, earthquakes of 13 September 1967, *Bull. Seis. Soc. Am.*, 71(1), 1-24.
- Minson, S. and D. Dreger (2007). Improved seismic moment tensor inversion, *Geophys J. Int.*
- Muller, G. (1973). Seismic moment and long-period radiation of underground nuclear explosions, *Bull. Seis. Soc. Am.*, 63(3), 847-857.
- Pechmann, J. C., W. R. Walter, S. J. Nava, and W. J. Arabasz (1995). The February 3, 1995 ML 5.1 seismic event in the trona mining district of southwestern Wyoming, *Seism. Res. Lett.*, 66, 25-34.
- Saikia, C. K. (1994). Modified frequency-wavenumber algorithm for regional seismograms using Filon's quadrature; modelling of Lg waves in Eastern North America, *Geophys. J. Int.*, 118(1), 142-158.
- Song, X. J., D. V. Helmberger and L. Zhao (1996). Broad-band modelling of regional seismograms; the basin and range crustal structure, *Geophys. J. Int.*, 125(1), 15-29.
- Taylor, S. R., (1994), False alarms and mine seismicity: an example from the Gentry mountain mining region, Utah, *Bull. Seism. Soc. Am.*, 84, 350-358.

Table 1. 1-D velocity model (Song et al., 1996)

Thick (km)	$V_\alpha$ (km/s)	$V_\beta$ (km/s)	$\rho$ (g/cc)	$Q_\alpha$	$Q_\beta$
2.5	3.6	2.05	2.2	100.0	40.0
32.5	6.1	3.57	2.8	286.0	172.0
$\infty$	7.85	4.53	3.3	600.0	300.0

Figure 1. Map with locations of the August 6, 2007 Crandall Canyon Mine event (red star) and September 1, 2007 event near Tremonton, Utah (orange star) and stations used in the inversion of the events (light blue and light red inverted triangles, respectively).

Figure 2. Best-fit mechanisms for the a) Crandall Canyon Mine event and b) Tremonton, Utah event. The principal axes and values are given along with the total scalar moment ( $M_0$ ) and moment magnitude ( $M_w$ ).

Figure 3. Data (black) and synthetics (grey) generated using the mechanism for the Crandall Canyon Mine event given in Figure 2a. To the left of each set of traces are the station, azimuth, and distance to the event. Traces are normalized to the maximum amplitude for a set of three-component recordings, where the amplitude is given in  $10^{-7}$  m on the last line to the left of the traces.

Figure 4. Data (black) and synthetics (grey) generated using the mechanism for the Tremonton event given in Figure 2b. To the left of each set of traces are the station, azimuth, and distance to the event. Traces are normalized to the maximum amplitude for a set of three-component recordings, where the amplitude is given in  $10^{-7}$  m on the last line to the left of the traces.

Figure 5. Comparison of potential mechanisms. Data (black) is compared with predicted waveforms for 4 mechanisms: Best-fit full solution (grey); Best-fit deviatoric solution (red); Horizontal crack (green); and a typical Basin & Range normal event (cyan).  $M_0$  (in  $10e^{14}$  N-m) and  $M_w$  are given below the focal mechanism plot for each type. To the left of each set of traces are the station, azimuth, and distance to the event. Traces are normalized to the maximum amplitude of the data, which is given in  $10^{-7}$  m on the last line to the left of the traces.

Figure 6. Radiation patterns of potential mechanisms. Polar plots where the radius is normalized to the maximum amplitude. The color of the pattern is related to the mechanism and the dashed or solid line represents positive and negative polarity for the maximum amplitude of a velocity trace at 300 km distance, respectively. There is no green pattern in the Love waves since the horizontal closing crack produces no SH energy along the horizontal. Stations are plotted at the appropriate azimuth.

Figure 7. Source-type plot after Hudson et al. (1989). Theoretical mechanisms are plotted with crosses and annotated. The September 1, 2007 event near Tremonton (orange star) plots near the DC mechanism. The August 6, 2007 Crandall Canyon Mine event (red star) plots in the general moment tensor space that defines a closing crack, or collapse. The event is located well outside the region occupied by tectonic earthquakes and near other collapse mechanisms (two mine collapses and one explosion cavity collapse) calculated by Ford et al. (2007). 95% confidence regions are also given, where the region for the Crandall Canyon Mine event is so small as to not be visible outside the symbol.

Figure 8. Source-type plot as a function of depth. Inset, variance reduction (VR) as a function of depth used to create the Green's functions. The color corresponds to VR and can be used to reference the depth from the inset plot. The star is the parameters given for a depth of 1 km.

Figure 9. Moment tensor decomposition where the diameter of the lower hemisphere projection is relative to the largest principal moment. a) The remainder mechanism ( $M^{\text{rem}}$ ) after subtraction of a horizontal crack that leaves no isotropic component and where the Poisson's ratio is given by the velocity model used to calculate the full moment tensor is decomposed to a CLVD and DC with the same T and P axes. The azimuth and plunge of the major vector dipole in the CLVD are  $229^\circ$  and  $48^\circ$ , respectively. b) The same remainder as in a) is decomposed to a major and minor DC. Source parameters of the major DC are strike =  $329^\circ$ , rake =  $-100^\circ$ , and dip =  $86^\circ$ . c) The remainder mechanism after subtraction of a horizontal crack that leaves no isotropic component and with a Poisson's ratio that gives a full DC remainder. Source parameters are strike =  $306^\circ$ , rake =  $76^\circ$ , and dip =  $16^\circ$ .

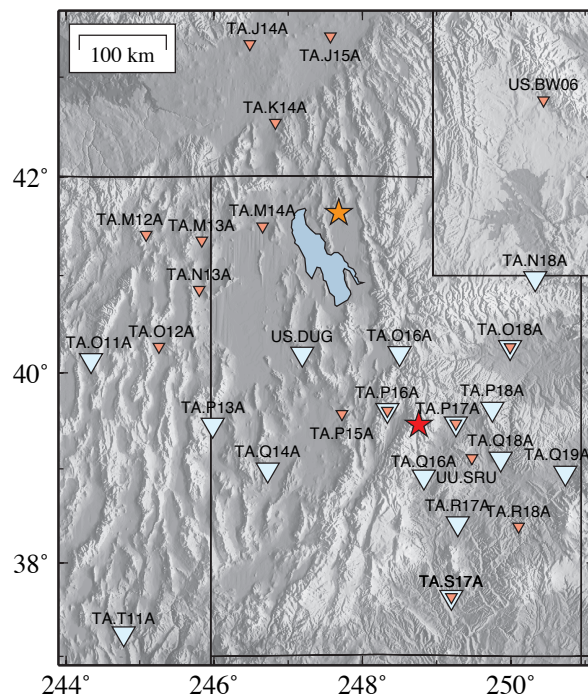
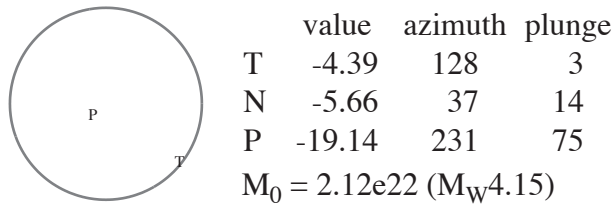


Figure 1. (1-column Color)  
 Ford et al., 2007  
 Version 2

a) Crandall Canyon Mine event (DC = 4%)



b) Tremonton event (DC = 90%)

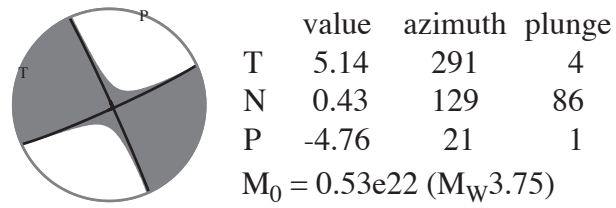


Figure 2. (1-column B/W)  
 Ford et al., 2007  
 Version 3

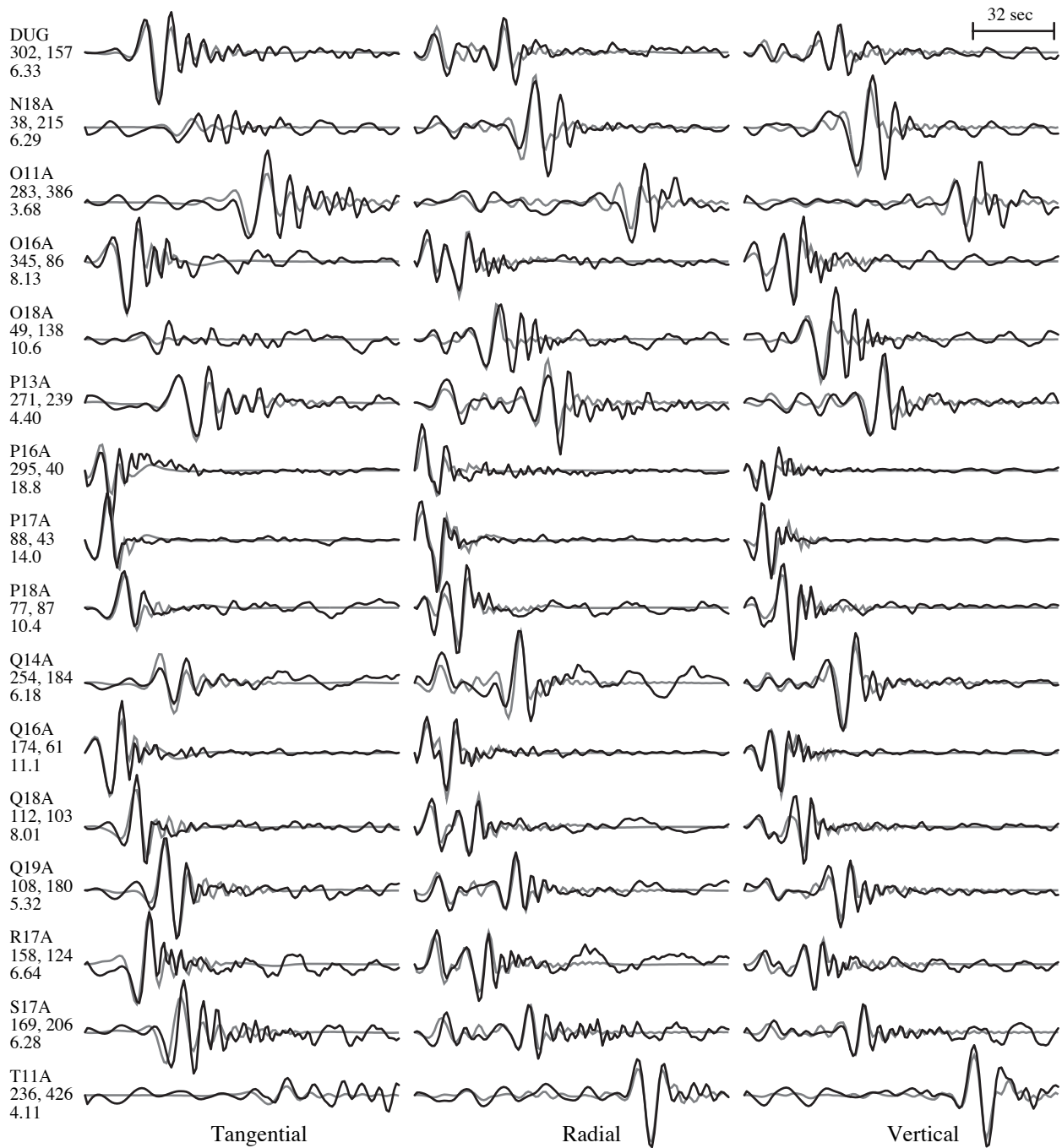


Figure 3. (2-column B/W)  
 Ford et al., 2007  
 Version 2

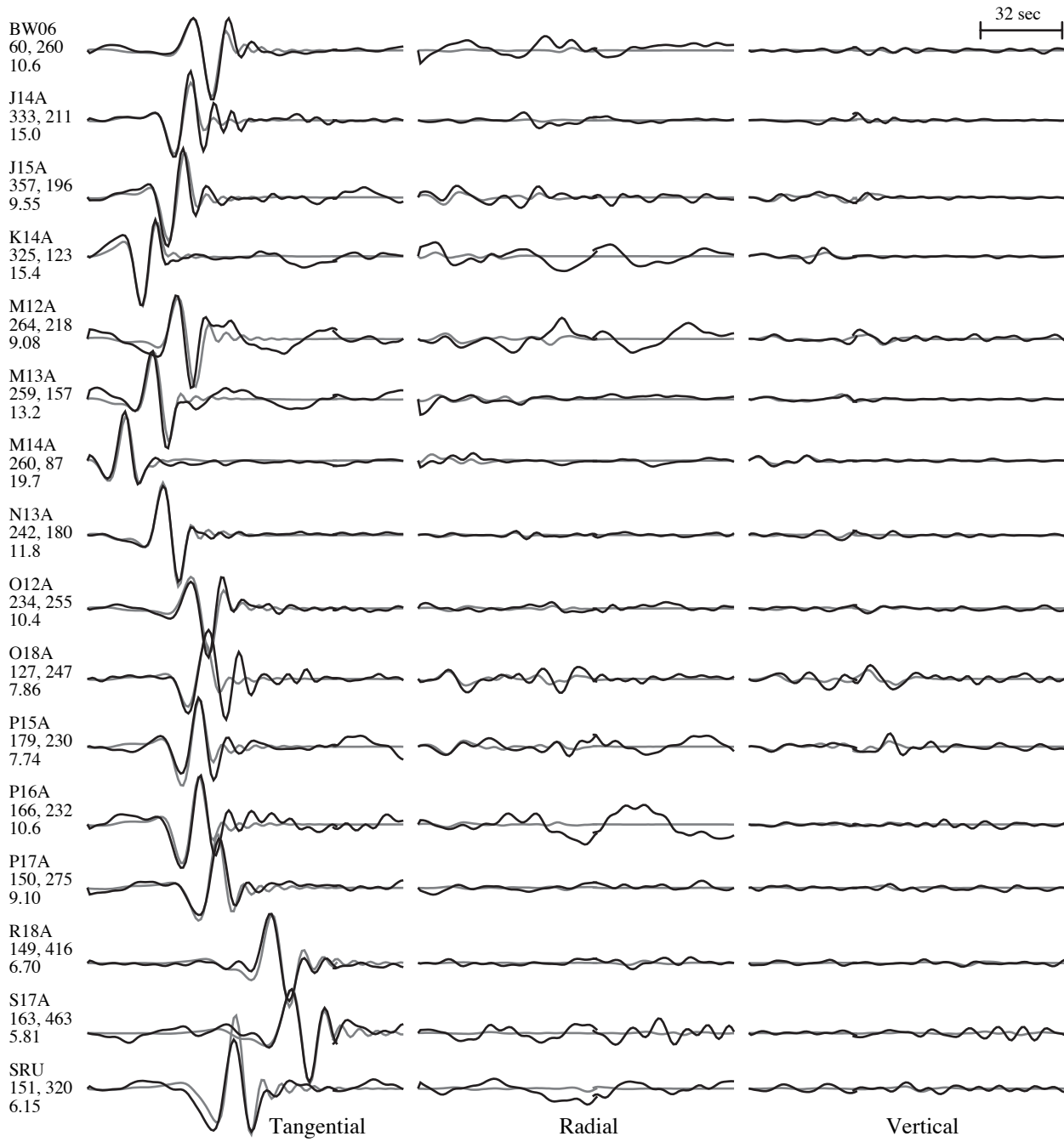


Figure 4. (2-column B/W)  
 Ford et al., 2007  
 Version 2

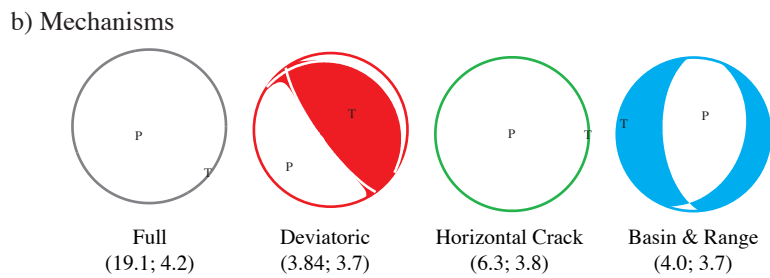
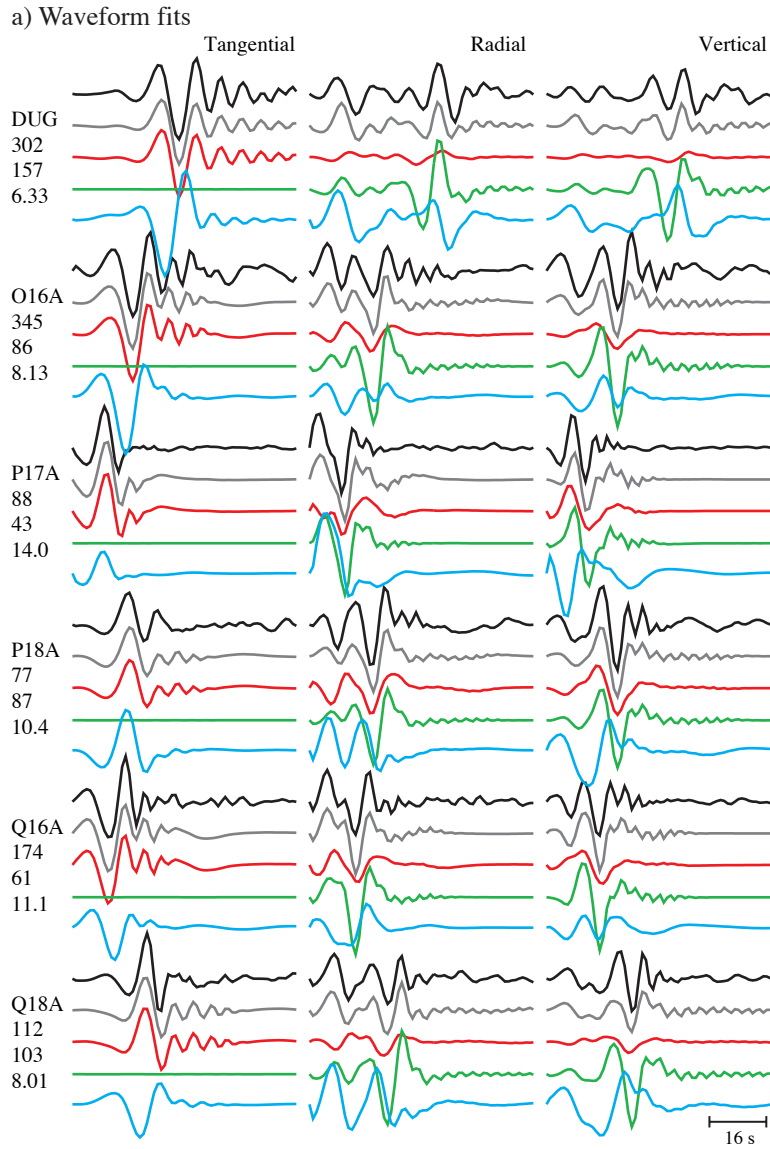
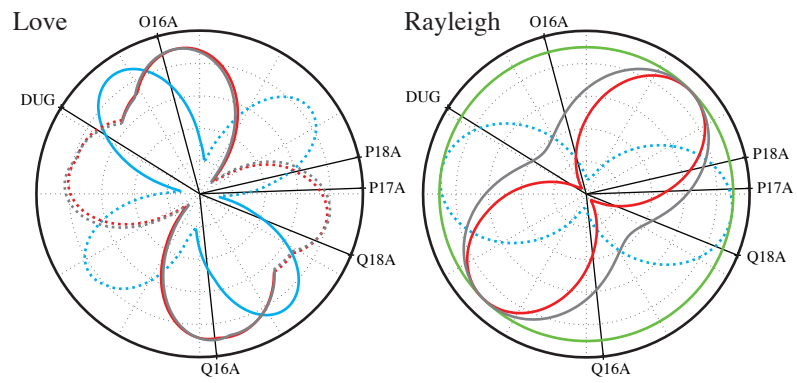


Figure 5. (2-column Color)  
Ford et al., 2007  
Version 3



Mechanisms: Full, Deviatoric, Horizontal Crack, Basin & Range

Figure 6. (1-column Color)  
 Ford et al., 2007  
 Version 3

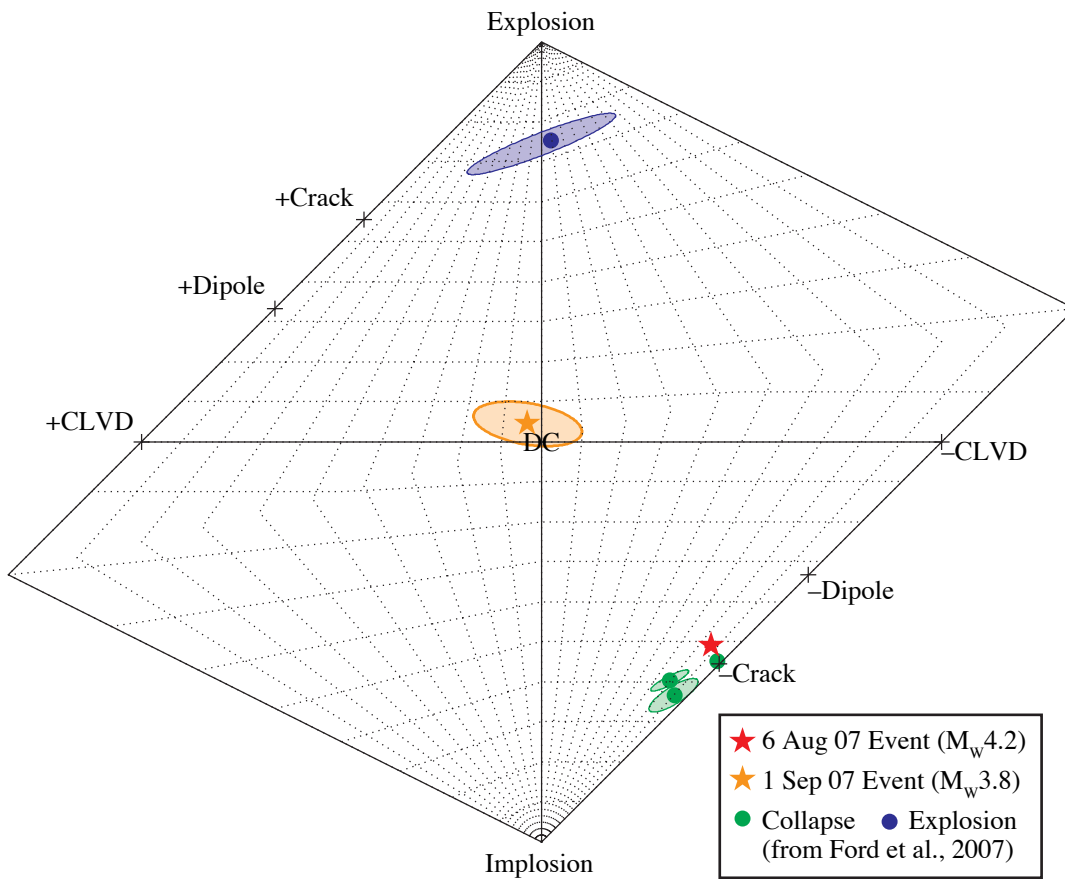


Figure 7. (2-column Color)  
 Ford et al., 2007  
 Version 2

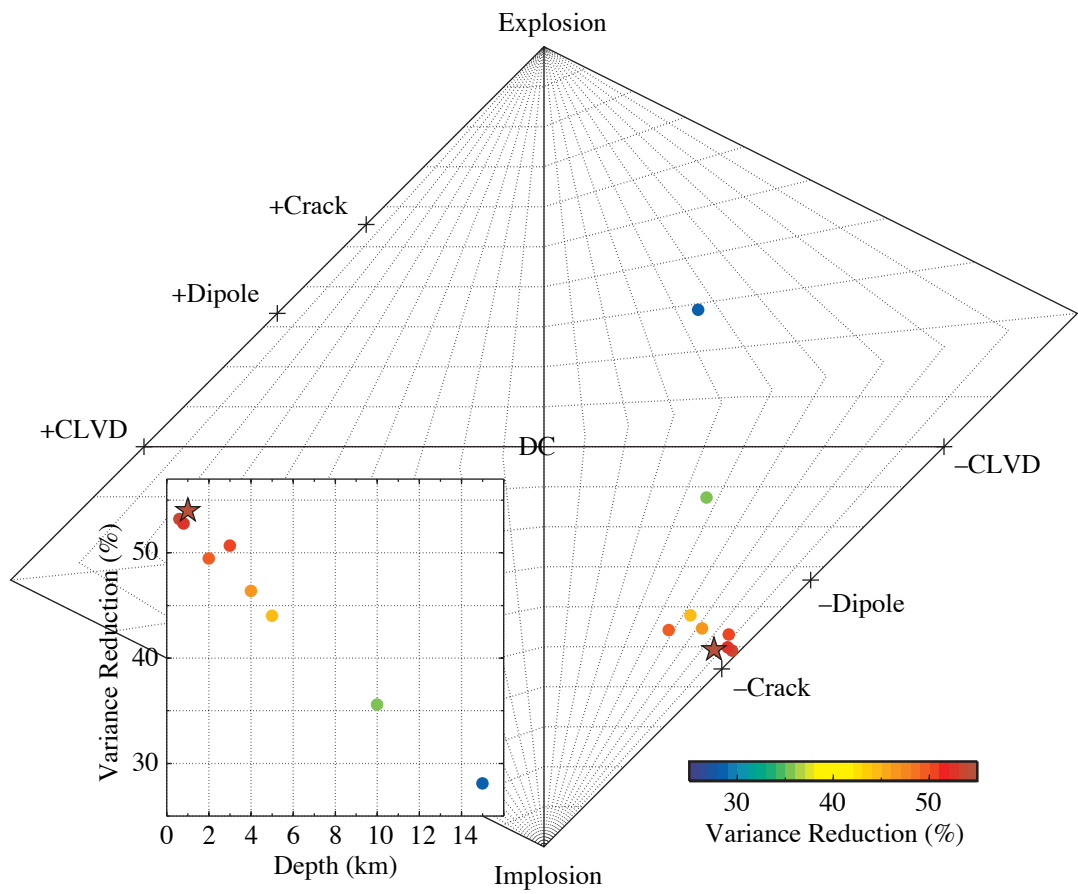


Figure 8. (1-column Color)  
 Ford et al., 2007  
 Version 2

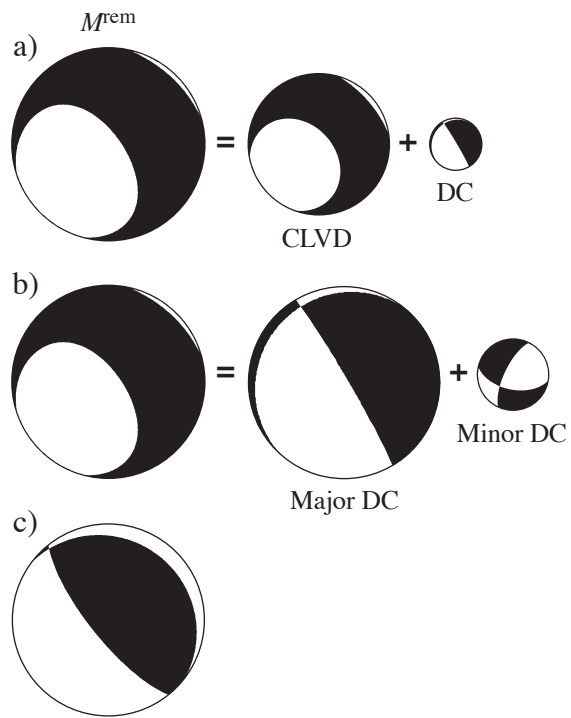


Figure 9. (1-column B/W)  
 Ford et al., 2007  
 Version 2